frontiers in Soil Science

TYPE Original Research
PUBLISHED 07 May 2026
DOI 10.3389/fsoil.2026.1780637

Check for updates

OPEN ACCESS

EDITED BY
Antonio Rafael Sánchez-Rodríguez,
University of Cordoba, Spain

REVIEWED BY
Muhammad Zeeshan Ul haq,
Hainan University, China
Wisnu Adi Wicaksono,
Graz University of Technology, Austria

*CORRESPONDENCE
Zhe Wang
wangzhe4048@163.com

RECEIVED 04 January 2026
REVISED 08 March 2026
ACCEPTED 20 March 2026
PUBLISHED 07 May 2026

CITATION
Wang Z, Mi X, Kang M, Yang X, Li W, Niu Y, Zhao Y and Li Y (2026) Reshaping the rhizosphere microbiome by humic acid enhances nutrient cycling and promotes *Salvia miltiorrhiza* growth. *Front. Soil Sci.* 6:1780637. doi: 10.3389/fsoil.2026.1780637

COPYRIGHT
© 2026 Wang, Mi, Kang, Yang, Li, Niu, Zhao and Li. This is an open-access article distributed under the terms of the Creative Commons Attribution License (CC BY). The use, distribution or reproduction in other forums is permitted, provided the original author(s) and the copyright owner(s) are credited and that the original publication in this journal is cited, in accordance with accepted academic practice. No use, distribution or reproduction is permitted which does not comply with these terms.

Reshaping the rhizosphere microbiome by humic acid enhances nutrient cycling and promotes *Salvia miltiorrhiza* growth

Zhe Wang[1]*, Xue Mi[1,2], Muxue Kang[1], Xinmeng Yang[1], Wan Li[1], Yuhua Niu[3,4], Yongping Zhao[1] and Yue Li[1]

[1]School of Biomedical and Food Engineering, Shangluo College, Shangluo, Shaanxi,, China, [2]Chinese Education Ministry's Key Laboratory of Western Resources and Modern Biotechnology, Key Laboratory of Biotechnology, Shaanxi Province, College of Life Sciences, Northwest University, Xi'an, China, [3]College of Chemistry and Chemical Engineering, Shaanxi University of Science and Technology, Xi'an, Shaanxi, China, [4]Shaanxi Humic Acid Ecological Remediation Engineering Research Center, Shaanxi University of Science and Technology, Xi'an, Shaanxi, China

Intensive cultivation of *Salvia miltiorrhiza* often leads to soil functional decline, compromising both yield and medicinal quality. Humic acid (HA) is recognized as a promising soil amendment, yet its integrated mechanisms within the plant-soil-microbe system remain unclear. Here, we conducted a pot experiment using soil from a *Salvia miltiorrhiza* monoculture system to evaluate the effects of three HA application rates (33.33, 16.67, and 8.67 mg/kg soil, designated as T1-T3, respectively) compared with conventional fertilization control (CK) on plant performance, soil properties, and the rhizosphere microbial functions. Our results revealed that HA application significantly enhanced plant biomass, with the T2 and T3 treatments increasing shoot biomass by 48.43% and 43.84%, and root biomass by 52.59% and 43.02%, respectively. HA application also significantly increased key bioactive compounds: tanshinone IIA rose by 81.46% (T2) and 74.39% (T3), and salvianolic acid B by 48.48% (T2) and 41.79% (T3). Soil enzyme activities were significantly enhanced, with β-glucosidase activity increasing by 70.60% and 68.27% at T2 and T3 treatments. The activity of β-N-acetylglucosaminidase and acid phosphatase rose by 4.22-fold and 1.37-fold under T2 treatment. Comparative metagenomic analysis between T2 and CK revealed that HA application altered microbial community composition; specific taxa, including *Luteitalea*, *Nitropira*, *Flavisolibacter*, *and Ferruginibacter*, were enriched in T2 treatment, with increases of 10.85%, 39.34%, 21.91%, 29.11%, respectively. Concomitantly, HA application significantly increased the abundance of functional genes associated with recalcitrant carbon decomposition (*abfA*, *faeB*, *manB*), organic carbon oxidation (*ilvE* and *pabBC*), nitrification (*amoA*, *amoB*, *amoC*, and *hao*), and phosphorus solubilization and mineralization (*gcd*, *pqqC*, *appA*, *phnP*, *and phoN*). Together, these findings show that HA enhances *Salvia miltiorrhiza* productivity and quality by modulating the soil-plant-microbe system, providing a mechanistic basis for HA-based strategies to improve soil quality that now warrant field-scale validation across diverse agroecological conditions.

KEYWORDS
humic acid, nutrient cycling, rhizosphere microbiome, salvia miltiorrhiza, soil enzymes activities

1 Introduction

The growing global demand for plant-derived medicinal products has intensified the cultivation of medicinal plants, often leading to soil quality decline that threatens both the sustainability and the quality of bioactive compounds (1). *Salvia miltiorrhiza* Bunge (*S. miltiorrhiza)*, a perennial herb of paramount importance in traditional Chinese medicine, is particularly susceptible to the adverse effects of continuous monoculture (2). In such systems, soil frequently experiences nutrient depletion, acidification, and structural deterioration (3, 4), which are closely linked to impaired plant growth and reduced accumulation of valuable secondary metabolites. Beyond these physicochemical constraints, soil quality decline encompasses a critical biological dimension. Intensive management practices, including chemical over-fertilization and diminished organic inputs, disrupt soil microbial communities and their essential functions in nutrient cycling (5). The rhizosphere microbiome, a critical interface for plant-microbe interactions, often undergoes significant structural and functional simplification under continuous cultivation, leading to a decline in the diversity and abundance of beneficial microorganisms (6). This dysbiosis undermines vital ecosystem services such as nitrogen fixation, phosphorus solubilization, and organic matter decomposition, thereby constraining nutrient availability and plant health (7).

Humic substances (HS), particularly humic acids (HA), have emerged as a promising strategy for rehabilitation (8). As complex organic molecules derived from the decomposition of plant and microbial residues, HA exert multifaceted benefits on soil systems (9–11). They improve soil structure, enhance cation exchange capacity, and chelate essential micronutrients, thereby increasing nutrient bioavailability (12, 13). Furthermore, HA acts as a potent bio-stimulant, exhibiting phytohormone-like activities that directly promote root development and modulate plant physicochemical processes (14, 15).

Critically, the efficacy of HA is closely related to its ability to modulate soil microbial communities. HA application can enhance microbial diversity and steer community composition toward beneficial taxa, including plant growth-promoting rhizosphere (PGPR) and arbuscular mycorrhizal fungi (AMF) (16). This restructuring enhances the functional capacity of the microbiome for nutrient transformation, primarily by stimulating the activity of key enzymes such as phosphatase and protease, which drive nitrogen mineralization and phosphorus solubilization (17, 18). HA may also contribute to a disease-suppressive soil environment by fostering beneficial microbial interactions and priming plant systemic resistance (19, 20).

While the benefits of HA are well-demonstrated in conventional agriculture, its potential to improve soil biological functions in medicinal plant systems remains underexplored. The quality of *S. miltiorrhiza* depends critically on its secondary metabolite content, which is highly sensitive to soil nutrient status and microbial health. We therefore hypothesize that HA amendment improving soil quality by reshaping the rhizosphere microbiome, thereby increasing nutrient use efficiency and promoting plant growth and quality. To test this, we conducted a comprehensive study with the following objectives: (i) characterize HA-induced shifts in rhizosphere microbial community composition, diversity, and functional potential; (ii) quantify changes in the activities of key enzyme activities involved in carbon, nitrogen, and phosphorus cycling; and (iii) assess the improvements in soil physicochemical properties, nutrient availability, and plant performance. By elucidating the mechanisms underlying HA-mediated improvements in soil-microbial-plant interactions, this study will offer a scientific basis for developing targeted strategies to enhance productivity and sustainability in medicinal plant agriculture.

2 Materials and methods

2.1 Experimental materials and design

A pot experiment was conducted from April to October 2024 at the campus of Shangluo College, Shaanxi Province, China. The experimental soil was collected from a field with a 3-year history of continuous *S.miltiorrhiza* cultivation. The soil had an organic matter content of 6.04g/kg, total nitrogen content of 0.53g/kg, total phosphorus content of 0.79 g/kg, an available phosphorus content of 12.73 mg/kg, and a pH of 8.3. The plant material used was authenticated *S.miltiorrhiza*, a Protected Geographical Indication (PGI) herb sourced from the Qinling Mountains. A liquid humic acid (HA) fertilizer (containing 30g/L free HA) was provided by the Ecological Engineering Centre at Shaanxi University of Science and Technology.

The experiment followed a completely randomized design with four replicates per treatment. All pots received a uniform base fertilizer (N-P_2O_5-K_2O = 15-15-15). Each pot (22cm diameter and 30cm height) was filled with 4.5kg of soil. A uniform base fertilizer (N-P_2O_5-K_2O = 15-15-15) was applied at 1.5 g per pot and thoroughly mixed into the soil before planting. Five uniform seedlings were transplanted in each pot, and thinned to three vigorous seedlings after emergence. Each pot represented an independent replicate, with a total of 4 replicates per treatment. Following a preliminary assessment of growth responses, three effective HA dilution levels were selected for detailed study: T1 (100-fold), T2 (200-fold), and T3 (400-fold), along with a no-HA control (CK) (21). Thirty days after seedling emergence, 500 mL of the corresponding HA dilution was applied to each pot via irrigation. Based on the stock concentration (30 g/L), the applied dilutions resulted in HA application rates of 0.15g/pot for T1, 0.075 g/pot for T2, and 0.0375g/pot for T3. Given that each pot contained 4.5kg of soil, these rates were equivalent to 33.3, 16.7, and 8.3mg HA per kg soil, respectively. The CK group received an equivalent volume of distilled water. All pots were maintained under consistent management conditions throughout the growing period (Apr to Oct 2024). The primary focus of the present study was to elucidate the underlying changes in rhizosphere microbial community structure, functional gene profile related to nutrient cycling, and their linkages to plant medicinal bioactive compounds, distinguishing it from prior assessments focused primarily on early growth parameters or basic soil fertility.

2.2 Plant and soil sampling and analysis

At harvest, plants were carefully uprooted and separated into aboveground (stems and leaves) and underground (roots) parts. Plant tissues from each pot were collected as a pooled sample to determine biomass, nutrient uptake, and bioactive compound content. For biomass measurement, samples were deactivated at 105°C for 30min and then dried at 75°C to constant weight to determine biomass dry weight. Total nitrogen (N) in plant tissue was assayed using the Kjeldahl method, and total phosphorus (TP) was analyzed via the molybdenum-antimony anti-spectrophotometric method. The uptake of N and P by *S.miltiorrhiza* was then calculated by multiplying the measured nutrient concentration by the corresponding biomass dry weight. The quantification of tanshiones IIA (T-IIA) and salvianolic acids B (S-AB) was performed according to a published HPLC protocol (22). Specifically, 0.2g of fine powdered root sample was extracted with 2mL of 70% methanol. Chromatographic separation was achieved on an UltiMate 3000 HPLC system using a ZORBAX SB-C18 column at 30°C. The PDA detector was set at 270 and 288 nm for monitoring tanshiones IIA and 288nm for salvianolic acids B, respectively.

For each pot, after gently shaking the roots to remove the loosely attached soil, the soil adhering to the roots was brushed off and retained as the rhizosphere soil (23). Each sample was subsequently homogenized and passed through a sieve (2mm) to remove plant and debris. A total of 16 rhizosphere soil samples (4 treatments × 4 replicates) were obtained. A portion was air-dried for baseline property evaluation, while another was flash-frozen in liquid nitrogen (N_2) and stored at -80 °C for DNA extraction and microbial community analysis. Fresh samples were transported and maintained at 4°C during transit, and stored under the same conditions for up to 24h before enzyme activity determination.

Soil organic carbon (SOC) was determined by potassium dichromate oxidation; NH_4^+-N and NO_3^-N contents were determined using a flow injection analyzer (AA3) after leaching with 1 mol/L KCl solution; Total nitrogen (TN) was determined using the Kjeldahl nitrogen method. Total phosphorus (TP) and available phosphorus (Olsen-P) were determined using the H_2SO_4-molybdenum antimony resistance method and the $NaHCO_3$ extraction method, respectively (24). The activities of Carbon-acquiring enzymes (β-glucosidase, βG; cellobiohydrolase, CBH), nitrogen-acquiring enzymes (β-1,4-N-acetylglucosaminidase, NAG), and phosphorus-acquiring enzymes (acid phosphatase, ACP) were determined using microplate-based fluorometric methods (25).

2.3 DNA extraction and metagenomic sequencing

To further investigate the microbiological mechanisms underlying the growth-promoting effects of HA on *S. miltiorrhiza*, the T2 group, which showed a favorable effect on plant performance and soil properties, was selected together with the control (CK), for subsequent metagenomic analysis. For each selected sample, total genome DNA was extracted from approximately 0.2g of frozen rhizosphere soil using the E.Z.N.A.® soil DNA Kit (Omega Bio-tek, US). DNA quality and concentration were assessed using a NanoDrop 2000 spectrophotometer and 1% agarose gel electrophoresis. Qualified DNA was fragmented to an average size of 350bp using a Covaris M220 ultrasonicator (Gene Company Limited, China) for paired-end library construction. Sequencing was performed on Illumina NovaSeq™ x Plus (Illumina Inc., San Diego, CA, USA) at Majorbio Bio-pharm Technology Co., Ltd (Shanghai, China).

Raw sequencing reads were trimmed with Fastp (v0.23.0) to remove adapters and low-quality reads (length < 50 pb or average quality values ≤ 20). After quality filtering, approximately 54.78 GB of clean reads were obtained from 8 samples, yielding 69.10-79.53 million high-quality reads per sample. Clean reads from each sample were assembled using MEGAHIT (version 1.1.2), generating 6,341,316 contigs. Contigs ≥ 300 bp were selected for further gene prediction and annotation. Open reading frames (ORFs) were predicted from the assembled contigs using Prodigal (v2.6.3), yielding 7,599,080 ORFs with a minimum length of 100 bp. These sequences were clustered with CD-HIT (v4.6.1), with an identity threshold ≥ 0.9 and a coverage threshold ≥ 0.9, resulting in a non-redundant gene catalog comprising 3,596,916 genes with an average length of 400.39 bp. Taxonomic annotation was performed by aligning the representative gene sequences (nucleotide) against the Non-Redundant (NR) Protein Database using DIAMOND (v2.0.13) in BLASTX mode with an E-value cutoff of 1×10^{-5}. Functional annotation was performed using DIAMOND BLASTX searches against the Kyoto Encyclopedia of Genes and Genomes (KEGG) database with the same E-value threshold. Clean reads from each sample were aligned to this non-redundant gene set using SOAPaligner (v2.21) with a sequence identity threshold ≥ 0.95. Only uniquely mapped reads were retained. Gene abundance was then calculated as reads per kilobase per million mapped reads (RPKM) to normalize for gene length and sequencing depth. The resulting RPKM values served as the basis for subsequent taxonomic and functional profiling.

2.4 Statistical analysis

One-way analysis of variance (ANOVA) was conducted using GraphPad Prism (version 10.4.1) to evaluate the effects of HA application on plant biomass, nutrient uptake, and soil physicochemical properties (n = 4 per treatment). To compare microbial community composition and functional gene profiles between T2 and CK groups, principal coordinates analysis (PCoA) based on Bray-Curtis distances was conducted, coupled with analysis of similarities (ANOSIM) with 999 permutations to test for statistical significance. Linear Discriminant Analysis Effects Size (LEfSe) was employed to identify differentially abundant microbial biomarker taxa between the two groups. This analysis was performed on the Majorbio Cloud Platform using the Wilcoxon rank-sum test for feature selection, followed by LDA to estimate effect sizes. To account for multiple comparisons, the Benjamini-Hochberg FDR correction was applied, and features with adjusted p-values < 0.05 and LDA score > 3.0 were considered statistically significant. Differentially abundant functional genes involved in C,

N, and P cycling between the two groups were identified using the Wilcoxon rank-sum test, with statistical significance set at adjusted p-values < 0.05. Key metabolism pathways were annotation and interpreted using the KEGG database, focusing on C metabolism (e.g., decomposition, oxidation, methanogenesis, acetate oxidation), N metabolism (e.g., nitrification, denitrification, organic N metabolism, nitrogen fixation, assimilatory nitrate reduction, and dissimilatory nitrate reduction), and P metabolism (e.g., organic P mineralization, inorganic P solubilization, polyphosphate degradation, regulatory and polyphosphate synthesis). All bioinformatic analyses were performed on the Majorbio Cloud platform (https://cloud.majorbio.com).

3 Results

3.1 Effects of HA on plant growth and soil physicochemical properties

Application of HA elicited a concerted improvement in the growth, nutrient acquisition, and medicinal quality of *S. miltiorrhiza* (Table 1). Plant biomass was significantly enhanced under HA treatments, with T2 and T3 increasing shoot biomass by 48.43% and 43.84%, and root biomass by 52.59% and 43.02%, respectively, compared to CK ($p < 0.01$). This growth was accompanied by improved nutrient uptake. Shoot N uptake was enhanced by 43.02% and 52.59% in T2 and T3 treatments, while P uptake increased by 65.80% and 58.35%, compared to CK. In roots, P uptake increased by 68.59% and 91.05% in T2 and T3 treatments, respectively ($p < 0.01$). Furthermore, the HA application significantly increased the contents of bioactive compounds. Compared to CK, the T2 and T3 treatments increased tanshinone IIA by 81.46% and 74.39%, and salvianolic acid B by 48.48% and 41.79%, respectively.

These plant improvements were closely linked to HA-induced changes in rhizosphere soil properties (Table 2). Compared with CK, the soil organic carbon (SOC) content increased 3.64-fold and 1.66-fold under T2 and T3 treatment, respectively ($p < 0.05$). Total nitrogen (TN) content increased by 21.44% and 20.01% in the same treatments ($p < 0.05$). Notably, the HA application dramatically enhanced mineral nitrogen availability, with NO_3^-N content increasing by 57.60% and 65.43%, and NH_4^+-N content increasing by 89.13% and 57.68% in the T2 and T3 treatments, respectively, compared to CK ($p < 0.01$). In contrast, total phosphorus (TP) content significantly decreased by 14.62% and 24.24% at T2 and T3 treatment, and Olsen-P content decreased by 19.91% and 15.20% compared to CK ($p < 0.01$).

3.2 Effects of HA on the enzyme activities related to nutrient metabolism

Humic acid amendments significantly enhanced the activities of key rhizosphere enzymes involved in nutrient cycling (Figure 1a). The T1 treatment elicited the strongest stimulation of carbon-acquiring enzymes, significantly increasing β-glucosidase (βG)

TABLE 1 Effects of HA on the biomass and nutrient uptake and medicinal compound contents of *S.miltiorrhiza*.

Treatments	CK	T1	T2	T3
SB (g/pot)	16.56 ± 1.82b	24.12 ± 1.33a	25.58 ± 1.99a	23.82 ± 1.77a
RB (g/pot)	25.44 ± 2.28c	29.38 ± 5.58bc	36.38 ± 3.06ab	38.82 ± 2.78a
SN (mg/pot)	24.84 ± 2.73b	36.18 ± 2.57a	36.87 ± 2.57a	35.73 ± 2.66a
RN (mg/pot)	34.85 ± 3.12c	40.25 ± 7.64b	49.84 ± 4.19a	53.18 ± 3.81a
SP (mg/pot)	18.05 ± 1.98b	23.39 ± 1.29b	29.92 ± 2.33a	28.58 ± 2.12a
RP (mg/pot)	31.29 ± 2.80b	35.84 ± 6.81b	52.75 ± 4.45a	59.78 ± 4.28a
T-IIA (mg/kg)	805.37 ± 27.56c	947.35 ± 32.47b	1461.47 ± 47.13a	1404.54 ± 75.34a
SA-B (mg/kg)	37.92 ± 3.37c	46.91 ± 1.12b	56.30 ± 4.48a	53.76 ± 1.62a

The values are expressed as mean ± SE (n = 4); Different lowercase letters indicate significant differences ($p < 0.05$) as determined by Tukey's honestly significant difference (HSD) test. SB, shoot biomass; RB, root biomass; SN, shoot N uptake; RN, root N uptake; SP, shoot P uptake; RP, root P uptake; T-IIA, tanshinone IIA; SA-B, salvianolic acid B.

TABLE 2 Effects of HA on the rhizosphere soil properties of *S. miltiorrhiza* (21).

Treatment	CK	T1	T2	T3
SOC (g/kg)	6.33 ± 0.88d	45.23 ± 5.19a	27.59 ± 4.00b	16.86 ± 0.97c
TN (g/kg)	0.68 ± 0.03b	0.84 ± 0.02a	0.83 ± 0.05a	0.82 ± 0.05a
TP (g/kg)	0.76 ± 0.03a	0.64 ± 0.03bc	0.65 ± 0.05b	0.57 ± 0.06c
Olsen-P (mg/kg)	11.05 ± 0.44a	10.72 ± 0.65a	8.86 ± 0.38b	9.37 ± 0.61b
NH_4^+-N (mg/kg)	7.96 ± 1.24b	14.77 ± 2.81a	15.07 ± 1.26a	12.56 ± 0.98a
NO_3^-N (mg/kg)	17.49 ± 2.54c	40.37 ± 9.54a	27.57 ± 2.84b	28.93 ± 2.81b

The values are expressed as mean ± SE (n = 4). Different lowercase letters on the same represented extremely significant differences at the level of $p < 0.05$. SOC, soil organic carbon; TN, total nitrogen; TP, total phosphorus; Olsen-P, availability Phosphorus; NH_4^+-N, ammonium nitrogen; NO_3^-N, nitrate nitrogen.

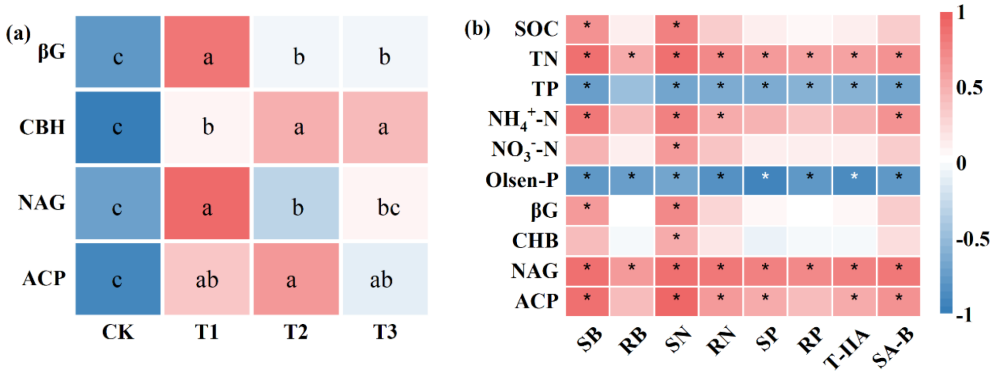


FIGURE 1
Heatmaps illustrate **(a)** treatment effects of HA on enzyme activities, and **(b)** correlations between soil properties and enzymes activities. The values are expressed as mean ± SE (n = 4). Different lowercase letters on the same represented extremely significant differences ($p < 0.05$). SOC, soil organic carbon; TN, total nitrogen; TP, total phosphorus; NH_4^+-N, ammonia nitrogen; NO_3^-N, nitrate nitrogen. *β*G, *β*-1,4-glucosidase; CBH, cellobiohydrolase; NAG, *β*-N-acetylglucosaminidase; ACP, acid phosphatase; SB, shoot biomass; RB, root biomass; SN, shoot N uptake; RN, root N uptake; SP, shoot P uptake; RP, root P uptake; T-IIA, tanshinone IIA; SA-B, salvianolic acid B. An asterisk (*) within a cell denotes a statistically significant correlation (p < 0.05)

and cellobiohydrolase (CBH) activities by 1.49-fold and 2.83-fold, respectively, compared to CK ($p < 0.05$). In contrast, the T2 treatment showed the most pronounced effects on the N and P acquisition, significantly boosting the activities of *β*-N-acetylglucosaminidase (NAG) and acid phosphatase (ACP) by 4.22-fold and 1.37-fold, respectively ($p < 0.05$). Correlation analysis further delineated the functional interplay between soil properties, enzyme activities, and plant performance (Figure 1b). Key plant growth parameters were positively correlated with TN, NAG, and ACP, while negatively correlated with TP and Olsen-P ($p < 0.05$), reinforcing the link between enhanced microbial nutrient mineralization and plant nutrient uptake. Furthermore, the content of specialized metabolites *tanshinone* IIA and *salvianolic acid* B showed significant positive correlation with the activities of ACP (Figure 1b, $\rho = 0.593$ and 0.528) and NAG (Figure 1b, $\rho = 0.575$ and 0.801, respectively, $p < 0.05$), suggesting a connection between microbially driven nutrient cycling and secondary metabolism.

3.3 Impact of HA on the structure and function of the rhizosphere microbiome

Given its favorable promotive effects on growth and nutrient uptake, the T2 treatment was selected for subsequent microbial analysis alongside the control (CK).

3.3.1 Microbial community diversity and composition

Humic acid application selectively modulated the rhizosphere microbiota, significantly increasing the bacterial Simpson index ($p = 0.038$), without altering other alpha-diversity indices (Supplementary Table 1). Beta-diversity analysis revealed a clear HA-induced structural shift in the bacterial community. Principal Coordinate Analysis (PCoA) at the phylum level showed distinct separation between CK and T2 groups (ANOSIM, $r = 0.26$, $p = 0.034$), with the first two coordinates accounting for 86.56% of the total variation (Supplementary Figure 1a). Consistent with this, genus-level PCoA also demonstrated significant community segregation (ANOSIM, $r = 0.448$, $p = 0.034$), accounting for 43.52% of the total variance (Figure 2a).

Taxonomic profiling revealed that the dominant bacterial phyla (relative abundance > 1%) were *Pseudomonadota*, *Actinomycota*, *Acidobacteriota*, *Bacteroidota*, *Chloroflexota*, *Nitrososphaerota*, *Gemmatimonadota*, *Cyanobacteriota*, and *Nitrospirota* (Supplementary Figure 1b). The LEfSe analysis further identified 5 phyla as key biomarkers in the T2 group, including *Acidobacteriota*, *Chloroflexota*, *Nitrospirota*, *Candiadtus_Aminicenantes* (Supplementary Figure 1c; LDA score > 3). Compared with CK, the relative abundances of *Acidobacteriota*, *Chloroflexota*, and *Nitrospirota* in the T2 treatment significantly increased by 9.60%, 7.92%, and 36.18%, respectively (Supplementary Figure 1d, $p < 0.05$). At the genus level, the dominant taxa included *Luteitalea*, *Sphingomonas*, *Nocardioides*, *Arthrobacter*, *Anaerolinea*, *Candidatus_Gaiellales*, *Chloracidobacterium*, *Bradyrhizobium*, *Blastococcus*, and *Terrimonas* (Figure 3c). The LEfSe analysis identified 6 genera as key biomarkers in the T2 treatment, such as *Luteitalea*, *Methylobacillus*, *Nitrospira*, *Flavisolibacter*, *Terrimonas*, and *Ferruginibacter* (Figure 3d; LDA score > 3). Compared to CK, the relative abundance of *Luteitalea*, *Nitropira*, *Flavisolibacter*, *and Ferruginibacter in* T2 treatment significantly increased by 10.85%, 39.34%, 21.91%, 29.11%, respectively (Supplementary Figure 2, $P < 0.05$).

3.4.2 Metabolic potential for carbon cycling

A total of 449 KEGG Orthologs (KOs) associated with microbial carbon turnover were identified and classified into 9 functional subgroups (Supplementary Figure 3). PCoA revealed a trend toward separation between the CK and T2 groups, although this difference was not statistically significant (ANOSIM, $r = 0.333$, $p = 0.071$). The first two axes explaining 67.00% of the total variation (Figure 2a). Dominant KOs in C-cycling, including K00249 (*acd*), K00626 (*atoB*), K00344 (*qor*), K03520 (*coxL*), K01895 (*acs*), K01681 (*ancA*), K00615 (*tktA*), and K05349 (*bglX*) (Figure 2b). Compared to CK, T2 treatment significantly increased the relative abundance

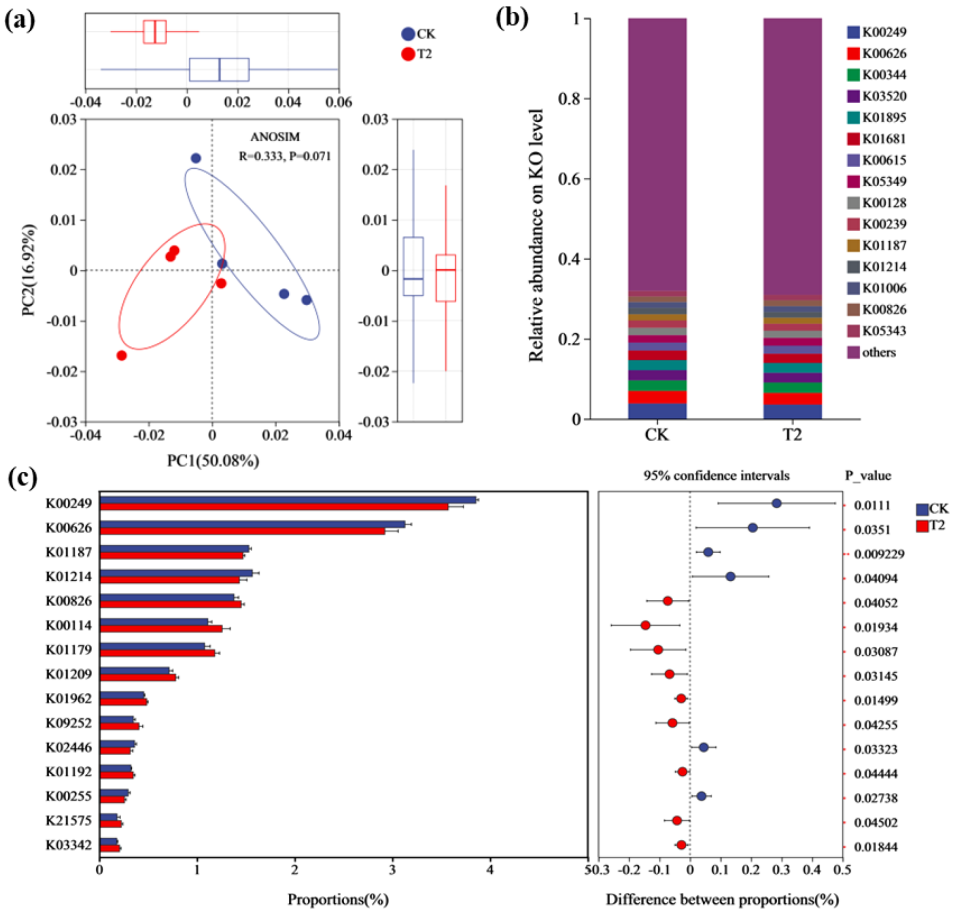


FIGURE 2
Comparative analysis of the carbon cycling potential between the two groups based on KEGG Orthology (KO) profiles. The values are expressed as mean ± SE (n = 4). **(a)** Principal coordinates analysis (PCoA) plot based on the Bray-Curtis distances, illustrating the dissimilarity in the overall nitrogen cycling functional potential between the groups; **(b)** Stacked bar chart representing the relative abundance of KO entries at the KO level for the two groups. **(c)** Bar chart showing the relative abundance of specific KOs, with statistically significant differences between two groups determined by the Wilcoxon rank-sum test at a statistical significance threshold of adjusted $p < 0.05$.

of K00826 (*ilvE*), K00114 (*exaA*), K01179 (E3.2.1.4), K01209 (*abfA*), K01962 (*accA*), K09252 (*FAEB*), K01192 (*manB*), and K03342 (*pabBC*) (Figure 2c, $p < 0.05$), while decreasing K00249 (*acd*), K00626 (*atoB*), K01187 (*malZ*), and K01214 (*terX*) (Figure 2c, $p < 0.05$).

3.4.3 Nitrogen metabolism potential

We identified 42 KOs involved in nitrogen metabolism, categorized into 5 functional groups (Figure 4a). PCoA showed a clear separation between the CK and T2 groups (ANOSIM, $r = 0.906$, $p = 0.034$), with 73.45% of variance explained (Figure 4b). Dominated N-cycling KOs included K01915 (*glnA*), K00265 (*gltB*), K00368 (*nirK*), K00372 (*nasC*, n*asA*), K00266 (*gltD*), K02575 (*narK*), and K00261 (*gdhA*) in both groups (Figure 4c). Compared to CK, the T2 treatment significantly increased the relative abundance of K00368 (*nirK*), K00261 (*gdhA*), K00370 (*narH*), K00376 (*nosZ*), K10944 (*amoA*), K10945 (*amoB*), K10946 (*amoC*), and K10535 (*hao*) (Figure 4d, $p < 0.05$), while it significantly decreased K00266 (*gltD*), K00362 (*nirB*), K00363 (*nirD*), and K00360 (*nasB*) (Figure 4d, $p < 0.05$).

3.4.4 Phosphorus metabolism potential

A total of 55 KOs involved in microbial P turnover were identified and classified into 5 functional categories (Figure 5a). PCoA revealed clear separation between the T2 and CK groups (ANOSIM, $r = 0.448$, $p = 0.034$), with the first two axes explaining 61.58% of the total variation (Figure 5b). The overall P-cycling KOs were dominated by K00117 (*gcd*), K01139 (*spoT*), K01126 (*glpQ*), K01524 (*ppx-gppA*), K02039 (*phoU*), K06167 (*phnP*), and K06137 (*pqqC*) in both treatments (Figure 5c). The T2 treatment significantly increased the relative abundance of K00117 (*gcd*), K06167 (*phnP*), K06137 (*pqqC*), K15986 (*ppaC*), K01093 (*appA*), and K09474 (*phoN*) (Figure 5d, $p = 0.012$, 0.001, 0.010, 0.027, 0.027, respectively), while K01139 (*spoT*), K02039 (*phoU*), K01126 (*glpQ*), and K01524 (*ppx-gppA*) showed higher abundance in the CK group (Figure 5d, $p = 0.045$, 0.035, 0.026 and 0.006, respectively).

10.3389/fsoil.2026.1780637

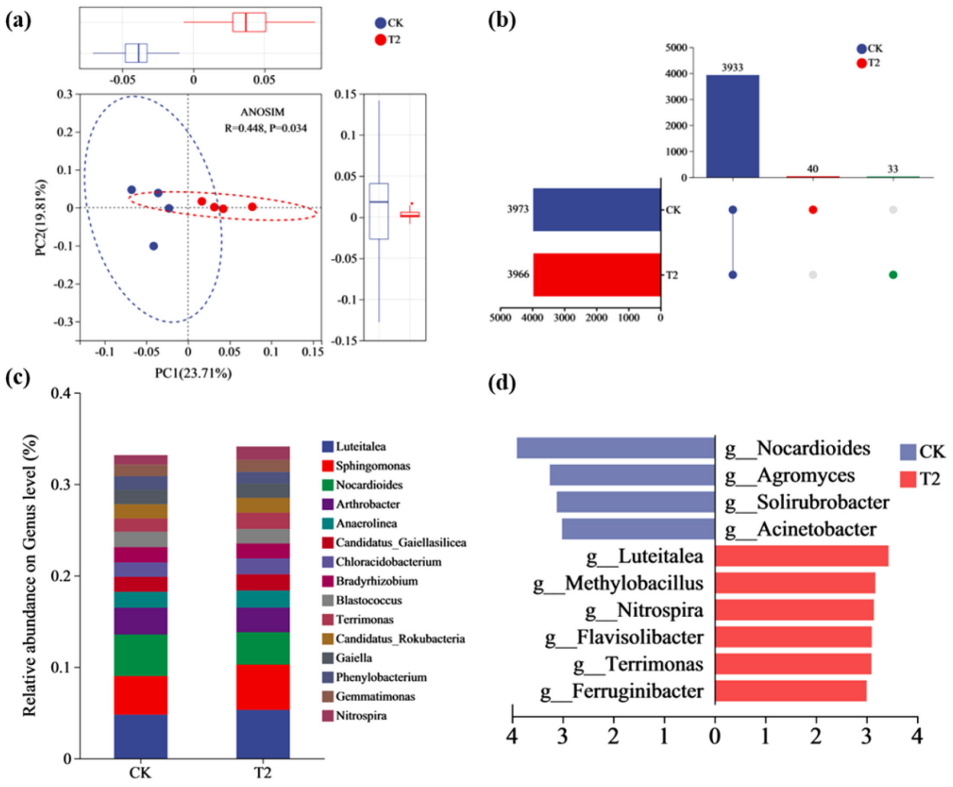


FIGURE 3
Microbial diversity and composition in the rhizosphere soil treated with HA at the genus level. The values are expressed as mean ± SE (n = 4). **(a)** Beta diversity represented by PCoA plot based on the Bray-Curtis distance in the bacterial genera; **(b)** Upset plot showing unique and shared genera in the two groups; **(c)** The relative abundance of top 15 bacterial genera across two groups **(d)** The linear discriminant analysis effects size (LEfSe) analysis showing the significantly different genera taxa (biomarkers) between the CK and T2 groups (LDA > 3 and $p < 0.05$).

4 Discussion

This study demonstrates that humic acid (HA) application effectively enhances the growth of *S.miltiorrhiza* compared with conventional chemical fertilization. We provide evidence that these benefits are from HA's coordinated influence on the soil-plant-microbe system, which improves rhizosphere nutrient cycling across multiple levels, from enzyme activity and community structure to function.

4.1 HA promotes plant growth and nutrient uptake

Our results demonstrated that HA significantly increased biomass accumulation and nutrient acquisition in *Salvia miltiorrhiza* (Table 1). We propose that these growth advantages extend beyond a direct nutritional supplement and are primarily mediated through an HA-induced priming effect on rhizosphere enzyme activities (Figure 1b), which act as key catalysts and indicators of soil nutrient cycling dynamics (26). The priming effect was evidenced by the significant increase in the activities of β-glucosidase (βG) and cellobiohydrolase (CBH) under HA treatment (Figure 1a). As an exogenous carbon source, HA likely serves as a metabolic trigger, stimulating cellulolytic bacteria to secrete these enzymes and thereby accelerate the decomposition of complex carbon polymers (27, 28). This response aligns with microbial energy-acquisition strategies, whereby labile carbon input stimulates investment in hydrolytic enzyme production to mine for more recalcitrant energy sources (29). The enhanced C turnover subsequently fuels the proliferation of N-cycling microorganisms. This consequent increase in β-N-acetylglucosaminidase (NAG) activity promotes the decomposition of chitin and other recalcitrant organic matter (29), facilitating the mineralization and release of plant-available NH_4^+-N and NO_3^- N (Table 2). The significantly positive correlation between plant biomass and NAG activity robustly supports this functional linkage (Figure 1b). In addition to microbial-mediated processes, the direct plant biostimulant of HA functions on plant physiology, which may further explain the enhanced nutrient uptake and growth observed in this study. Evidence indicates that HA can enhance plasma membrane H^+-ATPase activity, thereby increasing transpiration rates and facilitating mineral nutrient translocation (30), which could directly contribute to the improved nutrient acquisition we measured (Table 1) Furthermore, HA upregulates photosynthetic gene expression by activating key enzymes like Rubisco and modulating signaling molecules such as cytokinins and nitric oxide (31, 32). The stimulation of key nitrogen assimilation enzymes (e.g., nitrate reductase, glutamate dehydrogenase, and glutamine synthetase) creates a synergistic loop that synergizes with the rhizosphere priming effect to promote the overall nitrogen uptake and assimilation efficiency in our HA-treated plants.

Regarding phosphorus (P) cycling, HA enhances P availability through integrated enzymatic and abiotic pathways. It stimulates acid phosphatase (ACP) activity to mineralize organic P (33, 34), while its functional groups reduce P fixation via complexation, ion exchange,

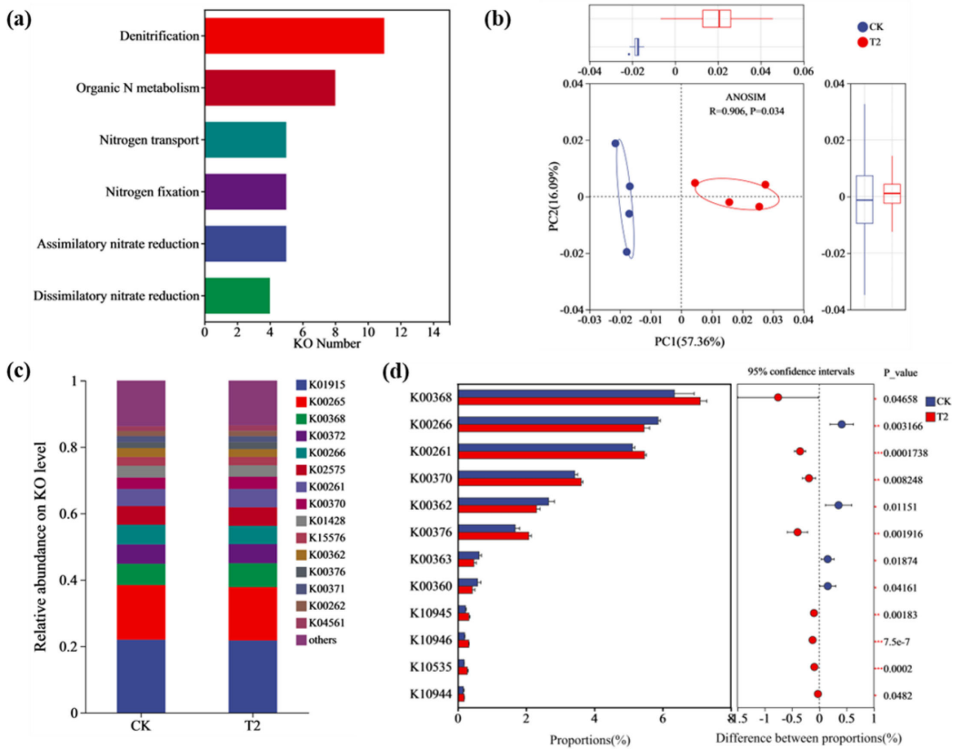


FIGURE 4
Comparative analysis of the nitrogen cycling potential between the two groups based on KO (KEGG Orthology) profiles. The values are expressed as mean ± SE (n = 4). **(a)** Bar Plot showing the number of KO identified associated with different nitrogen cycling processes in each group. **(b)** Principal coordinates analysis (PCoA) plot based on the Bray-Curtis distances, illustrating the dissimilarity in the overall nitrogen cycling functional potential between the groups; **(c)** Stacked bar chart representing the relative abundance of KO entries at the KO level for the two groups. **(d)** Bar chart showing the relative abundance of specific KOs, with statistically significant differences between two groups determined by the Wilcoxon rank-sum test at a statistical significance threshold of adjusted $p < 0.05$.

and competitive adsorption, thereby enhancing soil P availability (35, 36). The positive correlation between ACP activity and soil available P content underscores the central role of this enzyme in P mineralization (37). The observed negative correlation between plant growth and TP or Olsen-P can be explained by a dual mechanism (Figure 1b). First, HA established an integrated P mobilization system where ACP-mediated mineralization acts synergistically with enhanced inorganic P solubilization. Second, vigorous plant growth under HA treatment led to substantial P uptake, depleting soil P pools (Tables 1, 2). This combination of diversified acquisition pathways and intensified plant uptake accounts for the observed negative correlation (Figure 1b).

4.2 HA altered the rhizosphere microbiome for coupled nutrient cycling

Beyond stimulating enzymatic activity, HA application induced a profound reassembly of the rhizosphere bacterial community, selectively enriching specific taxa that collectively form a coordinated consortium for carbon (C), nitrogen (N), and phosphorus (P) cycling (Supplementary Figures 1c, 2d). This compositional shift reflects a microbial strategy oriented toward nutrient acquisition from complex organic sources. In the T2 treatment, oligotrophic taxa, such as *Acidobacteriota* and *Flavisolibacter*, which are known for decomposing recalcitrant polymers (e.g., cellulose, chitin) via extracellular enzymes like β-glucosidase (βG), were significantly increased, indicating enhanced potential for soil organic carbon mineralization (38, 39). Their prominence under T2 conditions suggests that the microbiome was functionally tuned to extract energy from persistent soil C pools, thereby supporting N and P transformation. Regarding N cycle, the T2 treatment significantly increased the abundance of *Nitrospira* (phylum *Nitrospirota*), a nitrifying genus responsible for oxidizing nitrite to nitrate, thereby enhancing soil N availability (40). Concurrently, the increase in *Luteitales* suggests a potential stimulation of dissimilatory nitrate reduction to ammonium (DNRA), a conservative pathway that retains N in a less mobile form (41). The co-enrichment of these organisms suggested that HA fosters a more efficient N cycling, increases N conservation, and reduces loss. Notably, T2 treatment also reinforced the functional coupling between N and P cycles. Beyond its direct role in chelating P-fixing cations, HA indirectly promoted P mobilization by stimulating nitrifiers such as *Nitrospira*. During nitrification, these organisms release organic acids (e.g., citric and oxalic acid) that effectively dissolve insoluble phosphates (e.g., Ca-P, Al-P, and Fe-P) (42–44). This establishes a cross-feeding coupling of nitrification and P solubilization, further reinforced by the enrichment of known P-solubilizing genera such as *Spingomonas* and *Luteitalea* (45, 46). The latter was identified as a dominant carrier of the *gcd* gene for P solubilization (47). Taxa such as *Ferruginibacter* may further contribute by reducing Fe^{3+} to soluble Fe^{2+}, liberating P from iron-phosphate complexes (48).

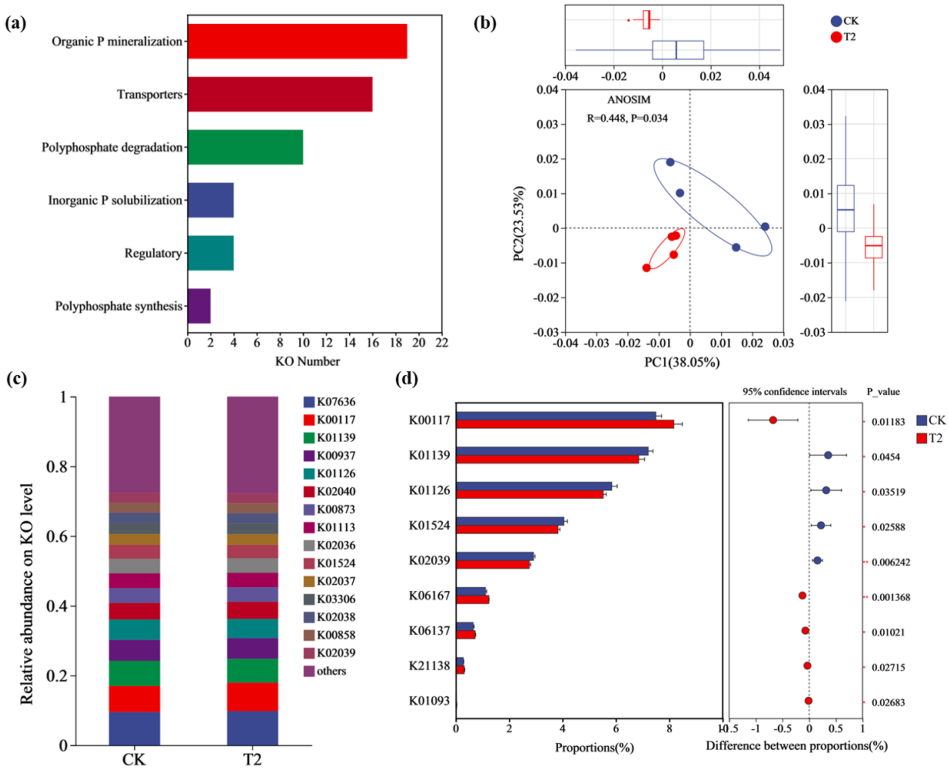


FIGURE 5
Comparative analysis of the phosphorus (P) cycling potential between the two groups based on KEGG Orthology (KO) profiles. The values are expressed as mean ± SE (n = 4). **(a)** Bar Plot showing the number of KO identified associated with different P-cycling processes in each group. **(b)** Principal coordinates analysis (PCoA) plot based on the Bray-Curtis distances, illustrating the dissimilarity in the overall P-cycling functional potential between the groups; **(c)** Stacked bar chart representing the relative abundance of KO entries at the KO level for the two groups. **(d)** Bar chart showing the relative abundance of specific KOs, with statistically significant differences between two groups determined by the Wilcoxon rank-sum test at a statistical significance threshold of adjusted $p < 0.05$.

4.3 HA steers microbial metabolic functions toward nutrient cycling

Metagenomic profiling revealed that HA application altered the functional potential of the rhizosphere microbiome, coordinating C, N, and P cycling processes that enhanced nutrient use efficiency. Specifically, HA amendment redirected microbial C metabolism toward the utilization of recalcitrant substrates. We observed a significant increase in genes involved in decomposing hemi-cellulosic polysaccharides and aromatic cross-linkages, including *abfA*, *faeB*, and *manB* (49), while genes for starch degradation, such as *malZ* and *terX*, were reduced (50) (Figure 2c). This shift from labile to recalcitrant C sources likely channels more C into microbial biomass and stabilization pathways. Concomitantly, the increase in *accA*, a key gene for CO_2 fixation (51), underscores a dual strategy wherein facilitated degradation of organic matter is coupled with autotrophic assimilation, jointly reinforcing soil C cycling. These alterations in C metabolism were coupled with modifications in the N cycling. The T2 treatment increased the abundance of *ilvE* and *pabBC* genes (Figure 2d), which link organic C oxidation to branched-chain amino acid transamination, thereby bridging C flux with N metabolism. The product of *ilvE* generates α-ketoglutarate and glutamate, suggesting that HA fosters an integrated C-N metabolic network that supports microbial energy efficiency. Furthermore, HA strongly enhanced the nitrification potential by upregulating the core genes encoding ammonia monooxygenase (*amoA*, *amoB*, and *amoC*) and hydroxylamine oxidoreductase (*hao*) (52–54). This coordinated enrichment, together with an increase in *gdhA* (encoding glutamate dehydrogenase) involved in ammonia assimilation (55), illustrates a comprehensive strategy to accelerate N transformation and boost N bioavailability (Tables 1, 2).

A pronounced genetic response was observed in the P cycle, confirming HA's role as a powerful activator of microbial P mobilization. HA application significantly increased the abundance of genes governing both inorganic P solubilization (*gcd*, *pqqC*) and organic P mineralization (*appA*, *phnP*, and *phoN*) (Figure 5d). The *gcd* gene encodes glucose dehydrogenase, which produces gluconic acid to chelate metal cations (e.g., Ca^{2+}, Fe^{3+}, and Al^{3+}) and releases plant-available phosphate (PO_4^{3-}) (56, 57). Its established correlation with soil available P confirmed its role as a key indicator of P activation (58). The *pqq* gene cluster (including *pqqC*) is essential for synthesizing the PQQ cofactor required for this reaction, establishing *pqqC* as a key marker of P-solubilizing bacteria (59, 60). Meanwhile, *appA*, *phnP*, and *phoN* encode phosphatases that hydrolyze organic phosphoesters (61–63), consistent with the observed increase in acid phosphatase activity (Figure 1a). Notably, the HA application decreased *spoT*, a central regulator of the bacterial stringent response typically activated under P limitation. Suppression of *spoT* implies that HA amendment fundamentally alleviates P limitation in the microbial community, reallocating cellular resources from stress response toward growth and P-mobilizing functions (64). Overall, HA acts as a metabolic modulator

that synchronizes C, N, and P cycling by selectively enriching key functional genes and taxa. This integrated strategy alters C metabolism toward recalcitrant substrates, enhances nitrification, and activates multiple P-solubilizing pathways, thereby establishing a coordinated nutrient cycling network that sustains microbial function and improves soil nutrient availability.

While this study provides mechanistic evidence for HA-mediated effects under controlled pot conditions, extrapolation to field-scale agricultural systems warrants caution. Environmental heterogeneity (e.g., climate, soil properties, native microbiota) may modulate HA efficacy in ways not captured here. The temporal dynamics of HA-microbiome interactions across growing seasons remain unknown. Future research should therefore prioritize multi-location field trials across diverse agroecological zones to validate whether these findings hold under realistic conditions and over multiple growing seasons. In particular, gradient field trials examining a range of application rates centered on the dose identified as optimal in this pot experiment would help establish empirically grounded recommendations for field use.

5 Conclusion

This study shows that humic acid (HA) application can positively influence plant growth and soil properties in *S. miltiorrhiza*. Among the three concentrations tested, the T2 treatment (16.67 mg/kg soil) exhibited the most promising effects on plant performance and nutrient availability. Comparative metagenomic analysis between T2 and control groups revealed distinct compositional profiles of the rhizosphere bacterial community, characterized by the enrichment of taxa implicated in decomposition and nutrient transformation, as well as increased abundance of functional genes related to recalcitrant carbon decomposition, organic carbon oxidation, nitrification, and phosphorus mobilization. These changes coincided with elevated enzyme activities and enhanced nutrient availability, which may have contributed to improved plant growth and accumulation of bioactive compounds. Our findings suggest that HA applied at an optimal concentration could modulate rhizosphere microbiome function, with potential implications for nutrient cycling in intensive agriculture. As this study was conducted under pot conditions, further field validation is needed to confirm these observations. This work provides a mechanistic foundation for developing HA-based strategies to enhance productivity and medicinal quality in intensive cultivation systems.

Data availability statement

The original contributions presented in the study are publicly available. This data can be found here: NCBI Sequence Read Archive (SRA), accession PRJNA1337597.

Author contributions

ZW: Funding acquisition, Writing – review & editing. XM: Data curation, Visualization, Writing – original draft. MK: Formal analysis, Methodology, Writing – original draft. XY: Formal analysis, Methodology, Writing – review & editing. WL: Conceptualization, Visualization, Writing – original draft. YN: Conceptualization, Funding acquisition, Writing – review & editing. YZ: Funding acquisition, Writing – review & editing. YL: Data curation, Methodology, Writing – original draft.

Funding

The author(s) declared that financial support was received for this work and/or its publication. This work was supported by the Natural Science Basic Research Program of Natural Sciences of Shaanxi Province (2023-JC-QN-0357); Shangluo Science and Technology R&D Program (2022-Y-0051): Shaanxi Provincial Technology Guidance Special Project (2023QYPY2-01); Research Start-up Fund for PhDs at Shangluo University (21SKY119); Key Research and Development Program Project of Shaanxi Province (2024NC-ZDCYL-02-11); Qinchuangyuan "Scientists + Engineers" Team Construction Project in Shaanxi Province (2023KXJ-009).

Conflict of interest

The author(s) declared that this work was conducted in the absence of any commercial or financial relationships that could be construed as a potential conflict of interest.

Generative AI statement

The author(s) declared that generative AI was not used in the creation of this manuscript.

Any alternative text (alt text) provided alongside figures in this article has been generated by Frontiers with the support of artificial intelligence and reasonable efforts have been made to ensure accuracy, including review by the authors wherever possible. If you identify any issues, please contact us.

Publisher's note

All claims expressed in this article are solely those of the authors and do not necessarily represent those of their affiliated organizations, or those of the publisher, the editors and the reviewers. Any product that may be evaluated in this article, or claim that may be made by its manufacturer, is not guaranteed or endorsed by the publisher.

Supplementary material

The Supplementary Material for this article can be found online at: https://www.frontiersin.org/articles/10.3389/fsoil.2026.1780637/full#supplementary-material.

References

1. Lu M, Powlson DS, Liang Y, Chadwick DR, Long S, Liu D, et al. Significant soil degradation is associated with intensive vegetable cropping in a subtropical area: a case study in southwestern China. *Soil*. (2021) 7:333–46. doi: 10.5194/soil-7-333-2021

2. Chen M, Yang G, Liu D, Li M, Qiu H, Guo L, et al. Inoculation with Glomus mosseae improves the growth and salvianolic acid B accumulation of continuously cropped Salvia miltiorrhiza. *Appl Sci*. (2017) 7:692. doi: 10.3390/app7070692

3. Zhang H, Zheng X, Wang X, Xiang W, Xiao M, Wei L, et al. Effect of fertilization regimes on continuous cropping growth constraints in watermelon is associated with abundance of key ecological clusters in the rhizosphere. *Agric Ecosyst Environ*. (2022) 339:1018135. doi: 10.1016/j.agee.2022.108135

4. Li H, Yuan G, Zhu C, Zhao T, Zhang R, Wang X, et al. Soil fumigation with ammonium bicarbonate or metam sodium under high temperature alleviates continuous cropping-induced Fusarium wilt in watermelon. *Sci Hortic*. (2019) 246:979–86. doi: 10.1016/j.scienta.2018.11.090

5. Garcia J, Kao-Kniffin J. Microbial group dynamics in plant rhizospheres and their implications on nutrient cycling. *Front Microbiol*. (2018) 11:1516. doi: 10.3389/fmicb.2018.01516

6. Chen Y, Du J, Li Y, Tang H, Yin Z, Yang L, et al. Evolutions and managements of soil microbial community structure drove by continuous cropping. *Front Microbiol*. (2022) 13:839494. doi: 10.3389/fmicb.2022.839494

7. Wang G, Ren Y, Bai X, Su Y, Han J. Contributions of beneficial microorganisms in soil remediation and quality improvement of medicinal plants. *Plants (Basel)*. (2022) 11:3200. doi: 10.3390/plants11233200

8. Ren H, Islam MS, Wang H, Guo H, Wang Z, Qi X, et al. Effect of humic acid on soil physical and chemical properties, microbial community structure, and metabolites of decline diseased bayberry. *Int J Mol Sci*. (2022) 23:14707. doi: 10.3390/ijms232314707

9. Canellas LP, Olivares FL, Aguiar NO, Jones DL, Nebbioso A, Mazzei P, et al. Humic and fulvic acids as biostimulants in horticulture. *Sci Hortic*. (2015) 196:15–27. doi: 10.1016/j.scienta.2015.09.013

10. Lumactud RA, Gorim LY, Thilakarathna MS. Impacts of humic-based products on the microbial community structure and functions toward sustainable agriculture. *Front Sustain Food Syst*. (2022) 6:977121. doi: 10.3389/fsufs.2022.977121

11. Ampong K, Thilakaranthna MS, Gorim LY. Understanding the role of humic acids on crop performance and soil health. *Front Agron*. (2022) 4:848621. doi: 10.3389/fagro.2022.848621

12. Mora V, Baigorri R, Bacaicoa E, Zamarreño AM, García-Mina JM. The humic acid-induced changes in the root concentration of nitric oxide, IAA and ethylene do not explain the changes in root architecture caused by humic acid in cucumber. *Environ Exp Bot*. (2012) 76:24–32. doi: 10.1016/j.envexpbot.2011.10.001

13. Zanin L, Tomasi N, Cesco S, Varanini Z, Pinton R. Humic substances contribute to plant iron nutrition acting as chelators and biostimulants. *Front Plant Sci*. (2019) 10:675. doi: 10.3389/fpls.2019.00675

14. Shah ZH, Rehman HM, Akhtar T, Alsamadany H, Hamooh BT, Mujtaba T, et al. Humic substances: Determining potential molecular regulatory processes in plants. *Front Plant Sci*. (2018) 13:263. doi: 10.3389/fpls.2018.00263

15. Zanin L, Tomasi N, Zamboni A, Sega D, Varanini Z, Pinton R. Water-extractable humic substances speed up transcriptional response of maize roots to nitrate. *Environ Exp Bot*. (2018) 147:167–78. doi: 10.1016/j.envexpbot.2017.12.014

16. Sun C, Bei K, Liu Y, Pan Z. Humic acid improves greenhouse tomato quality and bacterial richness in rhizosphere soil. *ACS Omega*. (2022) 7:29823–31. doi: 10.1021/acsomega.2c02663

17. Jindo K, Canellas L, Albacete A, Figueiredo dos Santos L, Frinhani Rocha R, Carvalho Baia D, et al. Interaction between humic substances and plant hormones for phosphorous acquisition. *Agronomy*. (2020) 10:640. doi: 10.3390/agronomy10050640

18. Xiong Q, Wang S, Lu X, Xu Y, Zhang L, Chen X, et al. The effective combination of humic acid phosphate fertilizer regulating the form transformation of phosphorus and the chemical and microbial mechanism of its phosphorus availability. *Agronomy*. (2023) 13:1581. doi: 10.3390/agronomy13061581

19. Jiang N, Wu M, Li G, Petropoulos E, Sun F, Wang X, et al. Humic substances suppress Fusarium oxysporum by regulating soil microbial community in the rhizosphere of cucumber (Cucumis sativus L.). *Appl Soil Ecol*. (2022) 174:104389. doi: 10.1016/j.apsoil.2022.104389

20. Rui R, Hei J, Li Y, Al Farraj DA, Noor F, Wang S, et al. Effects of humic acid fertilizer on the growth and microbial network stability of Panax notoginseng from the forest understorey. *Sci Rep*. (2024) 14:17816. doi: 10.1038/s41598-024-68949-9

21. Li Y, Li JL, Hu YX, Wang SH, Zhao YP, Wang Z. Effects of humic acid on the growth of Salvia miltiorrhiza and soil enzyme activity. *J Cold-Arid. Agric Sci*. (2025) 4:760–5. doi: 10.3969/j.issn.2097-2172.2025.08.008

22. Zhang C, Xing B, Yang D, Ren M, Guo H, Yang S, et al. SmbHLH3 acts as a transcription repressor for both phenolic acids and tanshinone biosynthesis in Salvia miltiorrhiza hairy roots. *Phytochemistry*. (2020) 169:112183. doi: 10.1016/j.phytochem.2019.112183

23. Zeeshan UHM, Gu G, Liu Y, Yang D, Yang H, Huang X, et al. ^{13}C labeling unveils soil and microbial changes in continuously cropped Pogostemon cablin. *Ecotoxicol. Environ Saf*. (2025) 303:118940. doi: 10.1016/j.ecoenv.2025.118940

24. Xu Y, Ge X, Zhou B, Lei L, Xiao W. Variations in rhizosphere soil total phosphorus and bioavailable phosphorus with respect to the stand age in Pinus massoniana Lamb. *Front Plant Sci*. (2022) 13:939683. doi: 10.3389/fpls.2022.939683

25. Chen Q, Liu Z, Zhou J, Xu X, Zhu Y. Long-term straw mulching with nitrogen fertilization increases nutrient and microbial determinants of soil quality in a maize–wheat rotation on China's Loess Plateau. *Sci Total. Environ*. (2021) 775:145930. doi: 10.1016/j.scitotenv.2021.145930

26. Daunoras J, Kacergius A, Gudiukaite R. Role of soil microbiota enzymes in soil health and activity changes depending on climate change and the type of soil ecosystem. *Biology*. (2024) 13:85. doi: 10.3390/biology13020085

27. Qin W, Feng J, Zhang Q, Yuan X, Ren F, Zhou H, et al. Different responses of priming effects in long-term nitrogen- and phosphorus-fertilized soils to exogenous carbon inputs. *Plant Soil*. (2024) 500:647–63. doi: 10.1007/s11104-024-06510-3

28. Xu J, Liu J, Fu Q, Zhang M, Guo B, Li H, et al. Soil carbon turnover and balance in the priming effects of basalt, montmorillonite, and kaolinite in a Luvisol soil. *J Soils. Sediments*. (2023) 24:732–43. doi: 10.1007/s11368-023-03676-8

29. De Mastro F, Brunetti G, Traversa A, Blagodatskaya E. Fertilization promotes microbial growth and minimum tillage increases nutrient-acquiring enzyme activities in a semiarid agro-ecosystem. *Appl Soil Ecol*. (2022) 177:104529. doi: 10.1016/j.apsoil.2022.104529

30. Rathor P, Upadhyay P, Ullah A, Gorim LY, Thilakarathna MS, Ahammed GJ. Humic acid improves wheat growth by modulating auxin and cytokinin biosynthesis pathways. *Ann Bot Plants*. (2024) 16:plae018. doi: 10.1093/aobpla/plae018

31. Shen J, Guo M, Wang Y, Yuan X, Wen Y, Song X, et al. Humic acid improves the physiological and photosynthetic characteristics of millet seedlings under drought stress. *Plant Signaling Behav*. (2020) 15:17742412. doi: 10.1080/15592324.2020.1774212

32. Chen Q, Qu Z, Ma G, Wang W, Dai J, Zhang M, et al. Humic acid modulates growth, photosynthesis, hormone and osmolytes system of maize under drought conditions. *Agric Water Manag*. (2022) 263:107447. doi: 10.1016/j.agwat.2021.107447

33. Ai L, Wu F, Fan X, Yang Y, Zhang Y, Zheng X, et al. Different effects of litter and root inputs on soil enzyme activities in terrestrial ecosystems. *Appl Soil Ecol*. (2023) 183:104764. doi: 10.1016/j.apsoil.2022.104764

34. Zhu H, Bing H, Wu Y, Sun H, Zhou J. Low molecular weight organic acids regulate soil phosphorus availability in the soils of subalpine forests, eastern Tibetan Plateau. *Catena*. (2021) 203:105328. doi: 10.1016/j.catena.2021.105328

35. Newcomb CJ. Humic matter in soil and the environment, principles and controversies. *Soil Sci Soc Am J*. (2015) 79:1520. doi: 10.2136/sssaj2015.0004br

36. Liu X, Zhao X, Lv J. Molecular characterization of size-fractionated humic acids derived from lignite and its activation of soil legacy phosphorus and Lactuca sativa growth-promoting performances. *ACS Omega*. (2023) 8:6838–346. doi: 10.1021/acsomega.2c07528

37. Chang Y, Wu Z, Peñuelas J, Sardans J, Chen Y, Jiang F, et al. Organic management improves soil P availability via increasing inorganic P solubilization in tea plantations. *Environ Technol Innovation*. (2025) 39:104223. doi: 10.1016/j.eti.2025.104223

38. Kielak AM, Barreto CC, Kowalchuk GA, van Veen JA, Kuramae EE. The ecology of Acidobacteria: Moving beyond genes and genomes. *Front Microbiol*. (2016) 7:744. doi: 10.3389/fmicb.2016.00744

39. Lian TX, Wang GH, Yu ZH, Li YS, Liu XB, Zhang SQ, et al. Bacterial communities incorporating plant-derived carbon in the soybean rhizosphere in Mollisols that differ in soil organic carbon content. *Appl Soil Ecol*. (2017) 119:375–83. doi: 10.1016/j.apsoil.2017.07.016

40. Song XL, Wang ZJ, Yin XW, Sun YL, Jang DJ, Hong SK. The impact of nitrogen deposition on nitrogen metabolism in ryegrass lawn with different soil nutrient levels. *Sci Rep*. (2025) 15:16755. doi: 10.1038/s41598-025-00578-2

41. She Y, Qi X, Sun S, Li Z. Biodegradable microplastics boost dissimilatory nitrate reduction to ammonium (DNRA) process contributing to ammonium nitrogen retention in farmland soils. *J Clean. Prod*. (2024) 438:140835. doi: 10.1016/j.jclepro.2024.140835

42. D'Acunto L, Andrade JF, Poggio SL, Semmartin M. Diversifying crop rotation increased metabolic soil diversity and activity of the microbial community. *Agric Ecosyst Environ*. (2018) 257:159–64. doi: 10.1016/j.agee.2018.02.011

43. Xu H, Liu W, He Y, Zou D, Zhou J, Zhang J, et al. Plant–root microbiota interactions in nutrient utilization. *Front Agric Sci Eng*. (2024) 12:16–26. doi: 10.15302/j-fase-2024595

44. Tao D, Gao Y. Advances on the strategies of soil phosphate solubilizing microorganisms to promote plant phosphorus uptake. *Acta Ecol Sin*. (2023) 43:4390–9. doi: 10.5846/stxb202111193253

45. Kim YJ, Park JY, Balusamy SR, Huo Y, Nong LK, Thi Le H, et al. Comprehensive genome analysis on the novel species Sphingomonas panacis DCY99 reveals insights into iron tolerance of ginseng. *Int J Mol Sci*. (2020) 21:2019. doi: 10.3390/ijms21062019

46. Asaf S, Khan AL, Khan MA, Al-Harrasi A, Lee IJ. Complete genome sequencing and analysis of endophytic Sphingomonas sp. LK11 and its potential in plant growth. *3 Biotech*. (2018) 8:389. doi: 10.1007/s13205-018-1403-z

47. Barquero MB, Garcia-Diaz C, Dobbler PT, Jehmlich N, Moreno JL, Lopez-Mondejar R, et al. Contrasting fertilization and phenological stages shape microbial-mediated phosphorus cycling in a maize agroecosystem. *Sci Total. Environ*. (2024) 951:175571. doi: 10.1016/j.scitotenv.2024.175571

48. Li MJ, Ye XX, Da YM, Sun QY, Zhou GW. Unveil of the role of fungal taxa in iron (III) reduction in paddy soil. *Front Microbiol*. (2023) 14:1334051. doi: 10.3389/fmicb.2023.1334051

49. Zhang Y, Li X, Xiao M, Feng Z, Yu Y, Yao H. Effects of microplastics on soil carbon dioxide emissions and the microbial functional genes involved in organic carbon decomposition in agricultural soil. *Sci Total. Environ*. (2022) 806:150714. doi: 10.1016/j.scitotenv.2021.150714

50. Du T, Hu Q, Mao W, Yang Z, Chen H, Sun L, et al. Metagenomics insights into the functional profiles of soil carbon, nitrogen, and phosphorus cycles in a walnut orchard under various regimes of long-term fertilisation. *Eur J Agron*. (2023) 148:126887. doi: 10.1016/j.eja.2023.126887

51. Zheng B, Zhu Y, Sardans J, Peñuelas J, Su J. QMEC: a tool for high-throughput quantitative assessment of microbial functional potential in C, N, P, and S biogeochemical cycling. *Sci China Life Sci*. (2018) 61:1451–62. doi: 10.1007/s11427-018-9364-7

52. Li J, Nedwell DB, Beddow J, Dumbrell AJ, McKew BA, Thorpe EL, et al. amoA gene abundances and nitrification potential rates suggest that benthic ammonia-oxidizing bacteria and not Archaea dominate N cycling in the Colne Estuary, United Kingdom. *Appl Environ Microbiol*. (2015) 81:159–65. doi: 10.1128/AEM.02654-14

53. Kaloterakis N, Giongo A, Braun-Kiewnick A, Rashtbari M, Zamberlan P, Razavi BS, et al. Rotational diversity shapes the bacterial and archaeal communities and confers positive plant-soil feedback in winter wheat rotations. *Soil Biol Biochem*. (2025) 203:109729. doi: 10.1016/j.soilbio.2025.109729

54. Zhang T, Sun Y, Parikh SJ, Colinet G, Garland G, Huo L, et al. Water-fertilizer regulation drives microorganisms to promote iron, nitrogen and manganese cycling: A solution for arsenic and cadmium pollution in paddy soils. *J Hazard. Mater*. (2024) 477:135244. doi: 10.1016/j.jhazmat.2024.135244

55. Guo X, Zhou X, Hale L, Yuan M, Feng J, Ning D, et al. Taxonomic and functional responses of soil microbial communities to annual removal of aboveground plant biomass. *Front Microbiol*. (2018) 9:954. doi: 10.3389/fmicb.2018.00954

56. Wang F, Zhang Y, Xia Y, Cui Z, Cao C. Soil microbial community succession based on PhoD and Gcd genes along a chronosequence of sand-fixation forest. *Forests*. (2021) 12:1707. doi: 10.3390/f12121707

57. Anantharaman K, Hausmann B, Jungbluth SP, Kantor RS, Lavy A, Warren LA, et al. Expanded diversity of microbial groups that shape the dissimilatory sulfur cycle. *ISME. J*. (2018) 12:1715–28. doi: 10.1038/s41396-018-0078-0

58. Liang JL, Liu J, Jia P, Yang TT, Zeng QW, Zhang SC, et al. Novel phosphate-solubilizing bacteria enhance soil phosphorus cycling following ecological restoration of land degraded by mining. *ISME. J*. (2020) 14:1600–13. doi: 10.1038/s41396-020-0632-4

59. Shi W, Xing Y, Zhu Y, Gao N, Ying Y. Diverse responses of pqqC- and phoD-harbouring bacterial communities to variation in soil properties of Moso bamboo forests. *Microb Biotechnol*. (2022) 15:2097–111. doi: 10.1111/1751-7915.14029

60. Meyer JB, Frapolli M, Keel C, Maurhofer M. Pyrroloquinoline quinone biosynthesis gene pqqC, a novel molecular marker for studying the phylogeny and diversity of phosphate-solubilizing pseudomonads. *Appl Environ Microbiol*. (2011) 77:7345–54. doi: 10.1128/AEM.05434-11

61. Sharma V, Kumar A, Archana G, Kumar GN. Ensifer meliloti overexpressing Escherichia coli phytase gene (appA) improves phosphorus (P) acquisition in maize plants. *Sci Nat*. (2016) 103:76. doi: 10.1007/s00114-016-1400-1

62. Wu X, Peng J, Liu P, Bei Q, Rensing C, Li Y, et al. Metagenomic insights into nitrogen and phosphorus cycling at the soil aggregate scale driven by organic material amendments. *Sci Total. Environ*. (2021) 785:147329. doi: 10.1016/j.scitotenv.2021.147329

63. Dai Z, Liu G, Chen H, Chen C, Wang J, Ai S, et al. Long-term nutrient inputs shift soil microbial functional profiles of phosphorus cycling in diverse agroecosystems. *ISME. J*. (2020) 14:757–870. doi: 10.1038/s41396-019-0567-9

64. Wang H, Chen J, Ruan Y, Sun W, Wang S, Wang H, et al. Metagenomes reveal the effect of crop rotation systems on phosphorus cycling functional genes and soil phosphorus availability. *Agric Ecosyst Environ*. (2024) 364:8886. doi: 10.1016/j.agee.2024.108886